JOURNAL OF PROPULSION AND POWER
Vol. 16, No. 6, November–December 2000

Determination of Triggering Condition of Vortex-Driven Acoustic Combustion Instability in Rocket Motors

Wen-Jing Wu* and Li-Chung Kung†
Chung Shan Institute of Science and Technology, Lung-Tan 325, Tao-Yuan, Taiwan, Republic of China

A method to determine the sufficient condition for the occurrence of acoustic combustion instability in solid rocket motors with slotted-tube grain is proposed. The condition is obtained by comparing the frequency of the shedding vortices at the entrance of the slots and the acoustic oscillation frequency in the upstream cylindrical port. To obtain the vortex shedding frequency, a transient flow analysis is conducted with the consideration of grain-surface regression. The method is assessed by analyzing five practical solid rocket motors employing slotted-tube grain in which acoustic combustion instability occurs in three cases, whereas the other two show no significant pressure oscillations. The results prove to be successful for all five motors. Furthermore, good agreement is obtained between the measurements and predictions, not only for the oscillatory frequencies but also for the occurrence time.

I. Introduction

COMBUSTION instability is widely encountered in the development of solid rocket motors. The spontaneous generation of pressure oscillations in rocket motors may cause significant operational problems such as change of thrust-time histories, additional acceleration loads on the motor components, and even failures of the motor systems if the oscillations overwhelm operational characteristics of the motor itself.

In general, the onset of combustion instability is determined by a balance between the sources and sinks of the oscillatory energy. The sink factors can be classified to be nozzle exhaust, particulate damping, flow-turning damping, suppression devices, and motions of the structure and propellant grain. On the other hand, the primary source factor is the response of the propellant-combustion zone to acoustic–pressure (pressure coupling) and acoustic–velocity (velocity coupling) oscillations. For certain modes of pressure oscillation, instability occurs when the energy sources exceed the sinks. Based on these concepts, a lot of effort[1–3] has been devoted to estimating the stability of combustion pressure. However, comparisons between the predictions and motor test data have shown significant discrepancies in many cases.[4] The poor agreement usually resulted from two causes. First, the individual energy source or sink factors cannot be determined accurately especially for practical rocket motors. For example, the mechanism of velocity coupling is somewhat controversial,[5] and how unsteady motor internal flow is established by propellant combustion is not clear.[6] A similar problem for energy sink terms also exists. Second, another oscillatory energy source factor due to vortex shedding in rocket motors was not considered in earlier works.[1–3] Flandro and Jacobs[7] first suggested that vortex shedding would be an additional potential source of acoustic energy in ducts and chambers. Brown et al.[4] experimentally examined vortex shedding phenomena in the full-scale Titan solid rocket motor (SRM) and found periodic flow separations could generate significant acoustic energy in the motors. They pointed out that the pressure oscillations occurred when the shedding frequency approximated the classical acoustic frequency. Experiments conducted by Culick and Magiawala,[8] Dunlap and Brown,[9] and Schadow and Wilson[10] also demonstrated coupling of the frequencies between the periodic vortex shedding and those of the acoustic modes of the chamber. Recently, in the analysis of Titan IV solid rocket motor (SRM) upgrade, Dotson et al.[11] found, even without inhibitors at the segment interfaces, vortices were shed around the cavity between the center and aft segments and resulted in pressure oscillations. Their observation also confirmed the oscillation amplitudes were largest when the frequencies of acoustic mode and the vortex shedding matched. It is known that the acoustic oscillations in a rocket chamber may be generated by various sources such as combustion, pressure, and flow disturbances. In general, most of the acoustic oscillations will be damped due to no continuous energy supply. However, in certain circumstances, the oscillatory energy will be sustained or even amplified if the acoustic waves are in phases with the periodic disturbances. The mechanism of energy transferred from the vortex to acoustic waves can be attributed to Rayleigh's criterion. Apparently, the occurrence of vortex shedding is inevitable in the motors with abrupt changes in the internal dimensions of rocket motors, for example, protruding of inhibitor rings, discontinuity of grain transition region, and other added devices such as baffles. The vortex shedding problem is most worrisome for the low-order pressure oscillation modes[12] and seems to be a dominant factor on the onset of acoustic combustion instability. Therefore, it is necessary to establish analyses capable of estimating combustion instability for rocket motors with vortex shedding in their internal flowfield.

The mechanism by which the energy is transferred from vortical to acoustic was concluded to be impingement of vortices on a solid surface at a suitable distance downstream of the shear layer origin.[11–14] In general, the solid surface may be the nozzle entrance or protruding inhibitors. Recent numerical analyses conducted by Vuillot[13] and by Kourta[14] demonstrated the flow structures with vortex rollup, convection, and impingement in SRMs. Vuillot[13] further illustrated an acoustic coupling model and suggested that one way to suppress vortex shedding driven oscillations is to reduce the shear layer critical frequency such that it is lower than the first acoustic mode frequency of the chamber. Based on this, the Strouhal number characterizing vortex shedding behavior was modified[11,13,14] to be

$$Sr_l = fl/U \tag{1}$$

in which l is the distance from the point of flow separation to the vortex impingement point, f is the vortex shedding frequency, and U is the freestream velocity. Instead of port diameter D_i or momentum thickness θ, application of length scale l in Eq. (1) implies that the coupling of vortex shedding and acoustic feedback behavior is determined by the flowfield downstream the separation point. Dotson et al.[11] argued that the freestream velocity U should be modified to be the vortex convection velocity by an artificial factor. However, none of the various definitions for Strouhal number could be safely used alone to correlate the results in consideration of the

Received 8 December 1997; revision received 20 August 1999; accepted for publication 21 October 1999.

*Assistant Scientist, Missile and Rocket Systems Research Division, P.O. Box No. 90008-15-1; wuwenj@ms29.hinet.net.

†Assistant Scientist, Missile and Rocket Systems Research Division.

oscillatory energy transfer.[13] Static test data employed in the present study also show (see Table 1) that no correlation exists between the observed pressure oscillation frequency and the first acoustic mode frequency based on the downstream characteristic length l (close to $L2$ in Table 1).

Another combustion instability phenomenon that merits attention is that of an axisymmetric ramjet combustor. In the numerical study of interaction between acoustic waves and vortex structures, Kailasanath et al.[15,16] indicated a strong coupling between the acoustic modes and the formation frequency of large vortical structures near the entrance to the combustion chamber. They also found that the entire flow oscillated at a low frequency that corresponded to that of a quarter-wave mode in the inlet. The frequency did not change with the length of the combustor. Another numerical modeling[17] of ramjet combustion instability also emphasized the importance of the inlet shear-layer instability. It is interesting that the same instability modes are obtained for both the solid rocket with slotted-tube grain as shown in Fig. 1 and the axisymmetric ramjet[15–17] in spite of some discrepancies between their geometries and flow characteristics. The upstream cylindrical port of a solid rocket chamber can be compared to the inlet of an axisymmetric ramjet with vortex-shedding onset at the end of the port and the inlet, respectively. The difference between these two cases is that the flow in the inlet is of constant flux (under a certain operating condition), and the length as well as the cross-sectional area of the inlet are not varied with time, whereas the flux in the upstream cylindrical port of a solid rocket chamber is a function of position and time because there is flow blowing from the periphery of the port, and in addition, the port length L and diameter Di vary with time due to grain-surface regression. Furthermore, the effects of vortex shedding on internal ballistics can be ignored in the earlier combustion period because the flow is confined in narrow slots, which hinders development of vortices. As the slot dimension becomes larger due to grain-surface regression, the vortex shedding phenomenon may play a more important role in combustion instability.

Table 1 Important parameters of test motors and their corresponding acoustic and instability frequencies

	Motor				
Parameter	1	2	3	4	5
L/D	3.29	8.98	3.68	9.91	4.52
$L1/L2$	1.63	0.44	1.45	2.84	2.48
Di/D	0.23	0.25	0.26	0.43	0.45
Slot number	3	4	4	5	5
Transition curve type	B	C	C	C	A
Weight fraction of aluminum in propellant	0.17	0.17	0.18	0.17	0.16
Fundamental acoustic frequency based on $2L$	342	150	400	251	675
Fundamental acoustic frequency based on $4L1$	276	245	338	170	474
Fundamental acoustic frequency based on $4L2$	450	108	491	482	1174
Observed pressure oscillation frequency	274	—	343	—	493

The slotted-tube grain is usually adopted to increase the burning surface of the booster phase or to attain the requirement of neutral burning. Figure 1 is a schematic of a slotted-tube grain, and Table 1 shows the corresponding dimensional parameters of five practical SRMs employed in present study. As mentioned, the abrupt changes in geometry at the transition region would generate vortex shedding. In general, three types of transition curves (A, B, and C, as shown in Fig. 1) can be found in motor design.

The acoustic waves propagated in SRMs are generally classified to be longitudinal modes and transverse modes. In the present study, the frequencies of the transverse mode are of the order of several thousands hertz, which would be damped by the particulate phase in the chamber. Therefore, only the longitudinal modes of acoustic waves are considered. As shown in Fig. 1, the axial characteristic lengths for slotted-tube-grain rocket chamber include L, $L1$, and $L2$ in which, during the combustion period, L remains constant while $L1$ and $L2$ vary slightly. In consideration of the acoustic mode based on the upstream cylindrical port length $L1$, the downstream end of the port (also the interface between $L1$ and $L2$) behaves like an open end such that the dominant acoustic mode of the upstream port would be the quarter-wave mode.[15] On the other hand, the acoustic mode based on the downstream characteristic length $L2$ would be more complex because the interface between $L1$ and $L2$ behaves as an open end for the central freestream, but as a fixed end for the flow in slots. Similar problem also exists for the acoustic mode based on the motor length L. Table 1 lists the analyzed frequencies based on these three lengths of the five test motors. Fortunately, for each case, it is not ambiguous to distinguish all of the first and second longitudinal modes from each other. As shown in Table 1, significant pressure oscillations were detected in static test data of motors 1, 3, and 5. It is found that the oscillatory frequencies correspond to those of quarter-wave mode in the upstream port (wavelength is equal to $4L1$ in Fig. 1).

According to the preceding discussion and the frequency analysis shown in Table 1, a sufficient condition for the vortex shedding driving combustion instability is reached when the frequencies between the acoustic field of quarter-wave mode in the upstream port and natural vortex shedding become close to each other. Thus, the attention is concentrated on the acoustic and the vortex shedding frequencies. By making use of the definition of Strouhal number based on momentum thickness

$$Sr_\theta = f\theta/U \tag{2}$$

the natural vortex shedding frequency at the entrance of the slotted-grain section can be obtained if the axial velocity distribution at the exit of the upstream cylindrical port is known. The value of Strouhal number Sr_θ for the axisymmetric mixing-layer mode is about 0.015 (Ref. 18), and its theoretical value has been identified to be 0.017 by Michalke.[19] Although the preceding value of Strouhal number is obtained in cold-flow measurements or simulation, it is still valid for reacting-flow conditions[15] (0.017 is used in present study).

The purpose of the present study is to develop a numerical method capable of determining the sufficient condition for the occurrence of acoustic combustion instability due to vortex shedding in the rocket

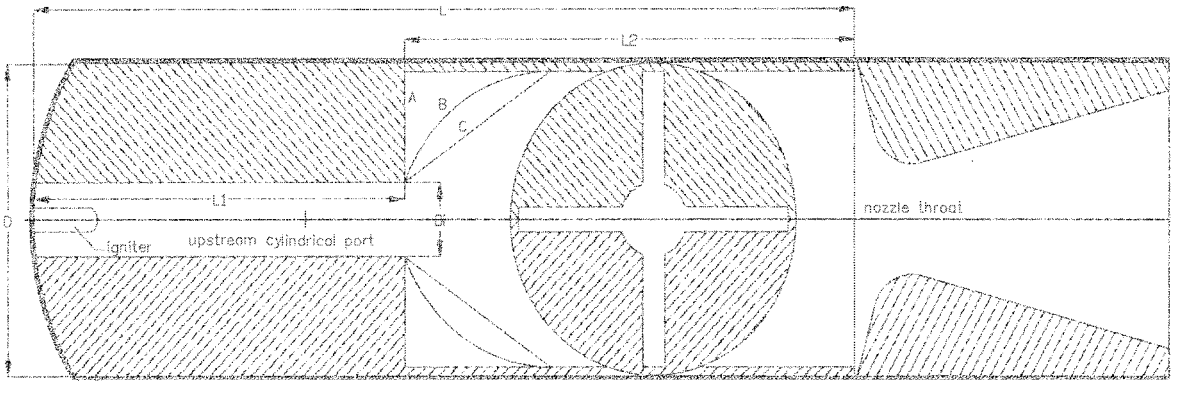

Fig. 1 Schematic SRM with slotted-tube grain.

motors. Static test data of the aforementioned five practical SRMs with slot-tube grain are analyzed.

II. Theoretical Model

Figure 1 is the schematic of an SRM with slot-tube grain, in which the transition curve and the number of slots (four in Fig. 1) may be changed to meet the design requirement. Because attention is paid to the flow profile at the exit of the upstream cylindrical port, it is reasonable to treat the flowfield as a homogeneous flow such that the energy equation and combustion details can be ignored in the following modeling. Furthermore, because of the simplicity of the flow (a pipe flow with wall blowing) the turbulent properties can be regarded as isotropic. In summary, the following assumptions are made:

1) The curvature of the head-end dome and the volume occupied by the igniter are ignored.

2) The flow temperature is assumed to be homogeneous and a function of specific impulse. The combustor pressure (or gas density) is also assumed to be constant (averaged value) for neutral burning design or two piecewise constants for the design with booster and sustainer phases. The burning rate (or grain-surface regression rate) is approximately constant under the limited pressure range such that the problem can be simplified to be an axisymmetric and transient one.

3) The flow follows the ideal-gas law.

4) The flow turbulence is described by the standard k–ε model.

According to the preceding assumptions, the governing equations consist of the conservation of mass, momentum in conjunction with the turbulence modeling equations for turbulence kinetic energy, and its dissipation rate. The ideal-gas law is employed to determine the flow density. The equations can be solved by the pressure-based algorithm[20] because of the low Mach flow characteristic in the computational domain.

Mass conservation:

$$\frac{\partial \rho}{\partial t} + \frac{\partial}{\partial x}(\rho u) + \frac{1}{r}\frac{\partial}{\partial r}(r\rho u) = 0 \tag{3}$$

Momentum conservation:

$$\frac{\partial(\rho u)}{\partial t} + \frac{\partial}{\partial x}(\rho u u) + \frac{1}{r}\frac{\partial}{\partial r}(r\rho v u) = \frac{\partial}{\partial x}\left(\mu_{\text{eff}}\frac{\partial u}{\partial x}\right) + \frac{1}{r}\frac{\partial}{\partial r}\left(r\mu_{\text{eff}}\frac{\partial u}{\partial r}\right) - \frac{\partial p}{\partial x} + \frac{\partial}{\partial x}\left(\mu_{\text{eff}}\frac{\partial u}{\partial x}\right) + \frac{1}{r}\frac{\partial}{\partial r}\left(r\mu_{\text{eff}}\frac{\partial v}{\partial x}\right) \tag{4}$$

$$\frac{\partial(\rho v)}{\partial t} + \frac{\partial}{\partial x}(\rho u v) + \frac{1}{r}\frac{\partial}{\partial r}(r\rho v v) = \frac{\partial}{\partial x}\left(\mu_{\text{eff}}\frac{\partial v}{\partial x}\right) + \frac{1}{r}\frac{\partial}{\partial r}\left(r\mu_{\text{eff}}\frac{\partial v}{\partial r}\right) - \frac{\partial p}{\partial r} - 2\mu_{\text{eff}}\frac{v}{r^2} + \frac{\partial}{\partial x}\left(\mu_{\text{eff}}\frac{\partial u}{\partial r}\right) + \frac{1}{r}\frac{\partial}{\partial r}\left(r\mu_{\text{eff}}\frac{\partial v}{\partial r}\right) \tag{5}$$

k Equation:

$$\frac{\partial(\rho k)}{\partial t} + \frac{\partial}{\partial x}(\rho u k) + \frac{1}{r}\frac{\partial}{\partial r}(r\rho v k) = \frac{\partial}{\partial x}\left(\frac{\mu_{\text{eff}}}{\sigma_k}\frac{\partial k}{\partial x}\right) + \frac{1}{r}\frac{\partial}{\partial r}\left(r\frac{\mu_{\text{eff}}}{\sigma_k}\frac{\partial k}{\partial r}\right) + G_k - \rho\varepsilon \tag{6}$$

ε Equation:

$$\frac{\partial(\rho\varepsilon)}{\partial t} + \frac{\partial}{\partial x}(\rho u \varepsilon) + \frac{1}{r}\frac{\partial}{\partial r}(r\rho v \varepsilon) = \frac{\partial}{\partial x}\left(\frac{\mu_{\text{eff}}}{\sigma_\varepsilon}\frac{\partial \varepsilon}{\partial x}\right) + \frac{1}{r}\frac{\partial}{\partial r}\left(r\frac{\mu_{\text{eff}}}{\sigma_\varepsilon}\frac{\partial \varepsilon}{\partial r}\right) + (c_1 G_k - c_2\rho\varepsilon)\frac{\varepsilon}{k} \tag{7}$$

Ideal-gas law:

$$p = \rho R T \tag{8}$$

where

$$G_k = \mu_t\left\{2\left[\left(\frac{\partial u}{\partial x}\right)^2 + \left(\frac{\partial v}{\partial r}\right)^2 + \left(\frac{v}{r}\right)^2\right] + \left(\frac{\partial v}{\partial x} + \frac{\partial u}{\partial r}\right)^2\right\}$$

$$\mu_{\text{eff}} = \mu + \mu_t, \qquad \mu_t = c_\mu \rho k^2/\varepsilon, \qquad c_\mu = 0.09, \qquad c_1 = 1.44$$

$$c_2 = 1.87, \qquad \sigma_k = 1.0, \qquad \sigma_\varepsilon = 1.3$$

The solution of Eqs. (2–8) yields a time-varying velocity profile at the upstream port exit. Thus, the momentum thickness can be obtained by use of the definition[18]

$$\theta = \int_0^{R_1} \frac{u}{U_c}\left(1 - \frac{u}{U_c}\right) \mathrm{d}r \tag{9}$$

and the natural vortex shedding frequency at the entrance of the slotted-grain section can be, in turn, determined from Eq. (2).

III. Numerical Method

The governing equations (3–7) in association with their corresponding boundary conditions are sequentially solved by fully implicitly schemes in time and space. Because the computational domain in the radial direction enlarges with time, a moving-boundary grid system based on grain-surface regression rate is employed. To keep the same grid spacing, the inner grid position is not adjusted during time marching, but an additional radial grid is added if the boundary grid width exceeds a certain value. On the other hand, the axial grid number may be reduced because the port length becomes slightly shorter during the combustion period. In the present study, the computational domain is discretized with a nonuniform, staggered 60×50 (axial by radial nodes) grid mesh. The time step is chosen to be 10^{-4} s to meet the requirement that the Courant number be less than one. Many iterations in each time step are required due to the fully implicit schemes. The convergence criterion based on the normalized mass residual is set to be 10^{-6}.

IV. Results and Discussion

As mentioned, data from five practical SRMs with slot-tube-grain design are employed to validate the present analysis. Table 1 summarizes several important parameters as well as the corresponding acoustic and instability frequencies of the five motors. The definition of dimensional parameters is given in Fig. 1. With quite different design requirements, the values of the dimensional parameter of the five test motors fall within a wide range. The motor length L varies from one to several meters, and the motor diameters are of the order of several hundred millimeters. It is noted that a high aluminum weight fraction in the propellant is employed for all of the test motors so that the high-frequency oscillations may be damped by the particulate phase in the chamber. Thus a sampling rate of 1000 Hz would be sufficient to resolve the frequencies of interest.

To compute the vortex shedding frequencies, as stated earlier, the computed flowfield includes only the upstream cylindrical port. However, the impedance at the discontinuity may change the vortex shedding frequencies. To investigate its effects, the computed flowfield has been purposely extended to cover the downstream region ($L2$) for the case of motor 1. The two computed curves of vortex shedding frequencies are shown in Fig. 2a in which vortex shedding frequency 1 is obtained from the simulation with the computed flowfield of only upstream port and vortex shedding frequency 2 represents the results from full flowfield calculation, respectively. It is found that the effects due to impedance at the discontinuity on vortex shedding frequency are insignificant because the discrepancies between the two curves are quite limited. As shown in Fig. 2a, the two curves of the vortex shedding frequencies 1 and 2 intersect with the acoustic frequency curve at the corresponding points of (0.29, 295) and (0.28, 294). Thus, for the sake of brevity, the computed

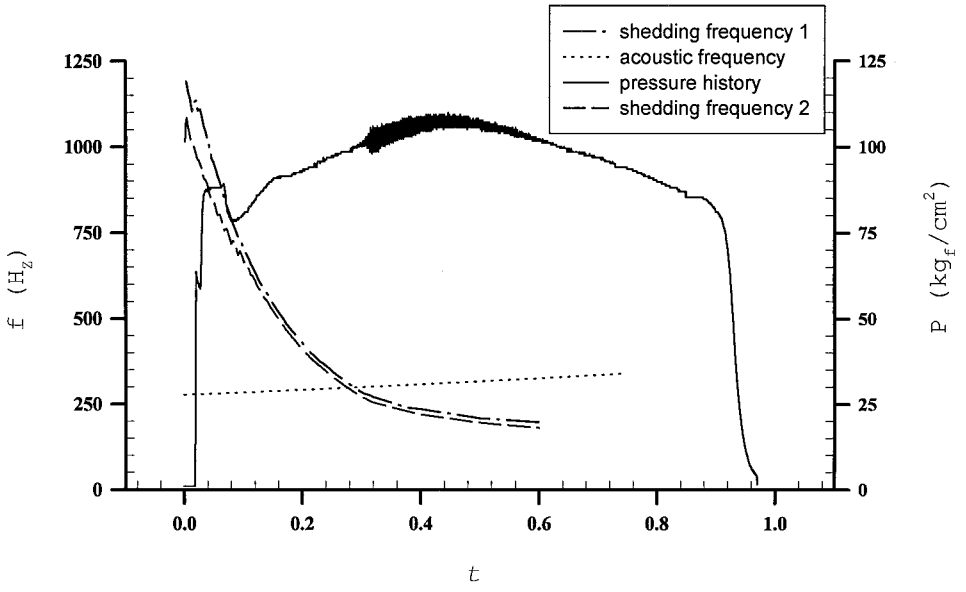

a) Pressure history and calculated frequencies

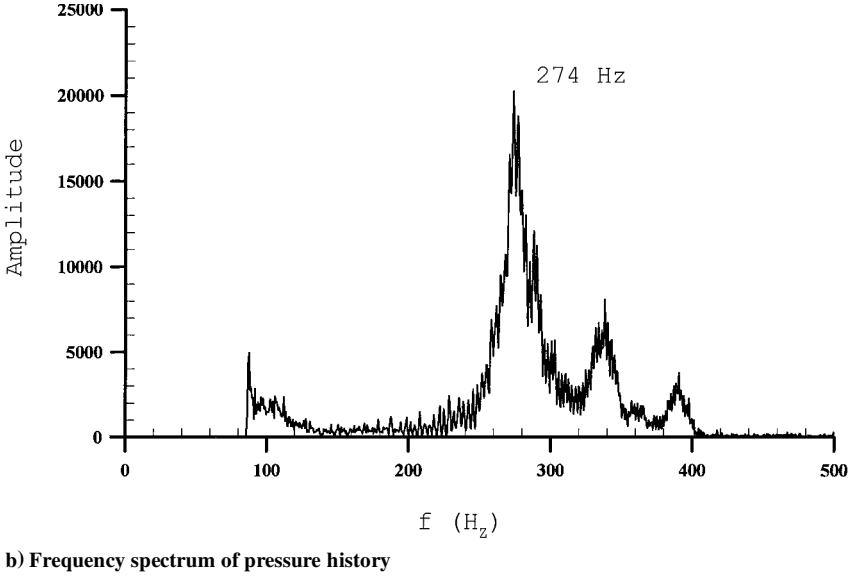

b) Frequency spectrum of pressure history

Fig. 2 Results of motor 1.

flowfield for the following cases of motors 2–5 includes only their own upstream ports (vortex shedding frequency 1).

Figure 2a also shows the measured head-end pressure history, the corresponding frequency spectrum, and the analytic results for motor 1. Note that t in the following figures is nondimensionlized by the corresponding motor's action time. As shown in Fig. 2a, significant pressure oscillation takes place at $t = 0.32$. The amplitude with respect to the average pressure is about 3%. The frequency spectrum shown in Fig. 2b exhibits a peak near 274 Hz, which agrees quite well with the fundamental acoustic frequency based on $4L1$ as shown in Table 1. Thus, we first employ the data of motor 1 to assess our method. In this case, single-phase thrust is designed such that the ballistic parameters are taken to be their average values, as mentioned in assumption 2. The grain blowing velocity and gas-phase density are calculated to be 7.5502 m/s and 8.3526 kg/m^3, respectively. Figures 3 and 4 show variation of the calculated axial centerline velocity and momentum thickness with respect to t. It is found

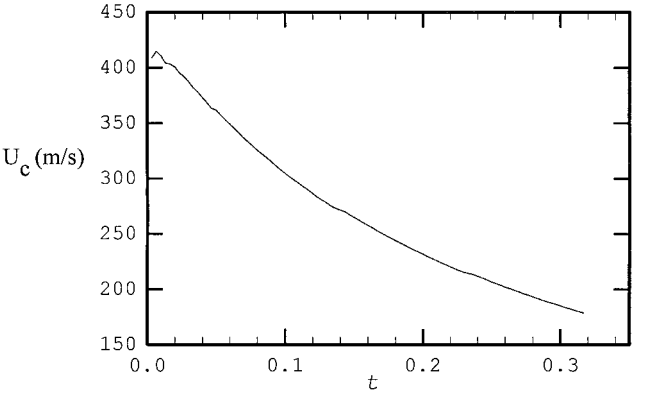

Fig. 3 Calculated axial centerline velocity at the slot entrance of motor 1.

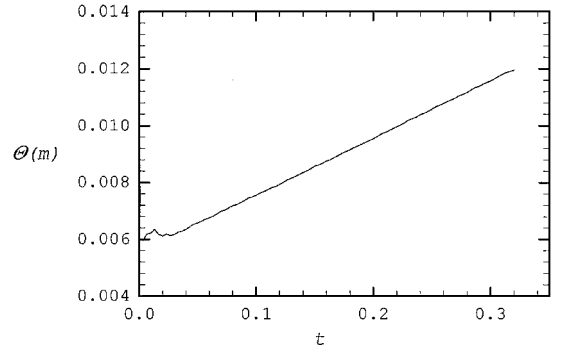

Fig. 4 Calculated momentum thickness at the slot entrance of motor 1.

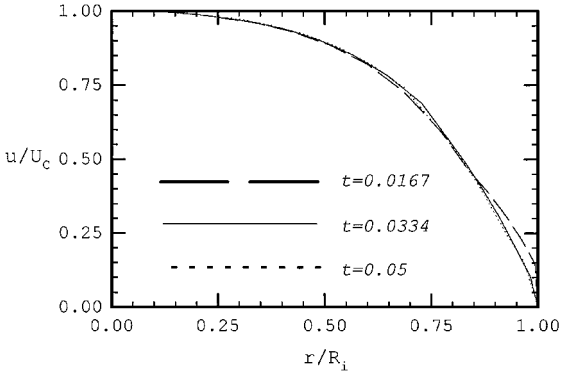

Fig. 5 Calculated axial velocity profiles at the slot entrance of motor 1.

that the momentum thickness increases almost linearly with time except at the beginning. This is because the upstream port diameter expands linearly due to the constant burning rate assumption, and similarity between the velocity profiles is reached after a short period, as shown in Fig. 5. The calculated centerline axial velocity at the port exit (see Fig. 3) becomes approximately inversely proportional to t. The reason for this relation is, during grain-surface regression, the burning surface is proportional to the port diameter but the port cross-sectional area is proportional to the square of the diameter.

After the momentum thickness and central axial velocity at the entrance of the slotted-grain section have been found, it is easy to obtain the natural vortex shedding frequency from Eq. (2). As shown in Fig. 2a, the calculated natural vortex shedding frequency decreases rapidly. The dashed line in Fig. 2a represents the calculated acoustic frequency based on the quarter-wave mode in the upstream port. A slight increase of the acoustic frequency can be found because the port length becomes shorter during combustion. The two frequency curves (vortex shedding frequency 1 and acoustic frequency) intersect at $t = 0.29$ and $f = 295$ Hz, which is close to the measured result, that is, $t = 0.32$ and f near 274 Hz. Kailasanath et al.[15,16] concluded that vortex shedding would be sustained in the frequency of acoustic oscillation if both frequencies become close to each other. This is why the measured instability can sustain for a certain period (from about $t = 0.3$ to 0.5) in spite of the continuous reduction of the predicted natural vortex shedding frequency. The simulation implies strong interactions between the acoustic wave and vortex shedding if the vortex shedding frequency matches that of the acoustic oscillation. In other words, as a vortex sheds from the entrance of slots, there follows a pressure disturbance propagating upstream into the cylindrical port with sound speed. After propagation through one wavelength, the disturbance is just in phase with the shedding of the

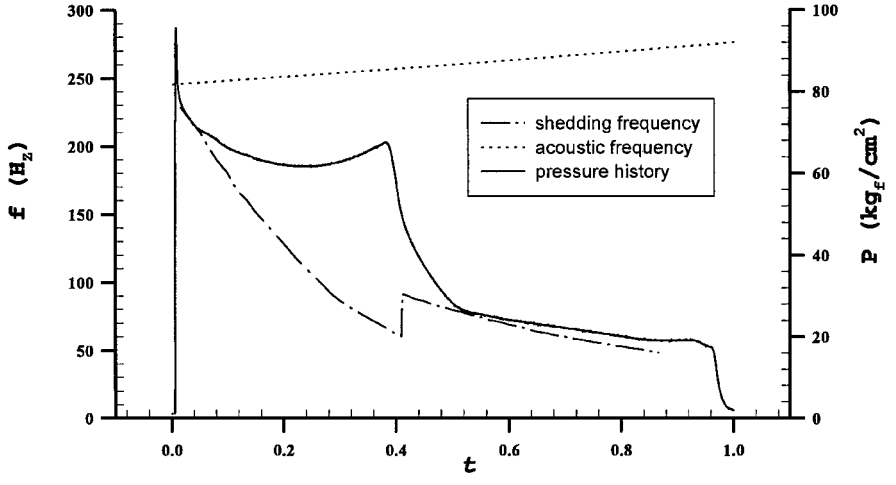

a) Pressure history and calculated frequencies

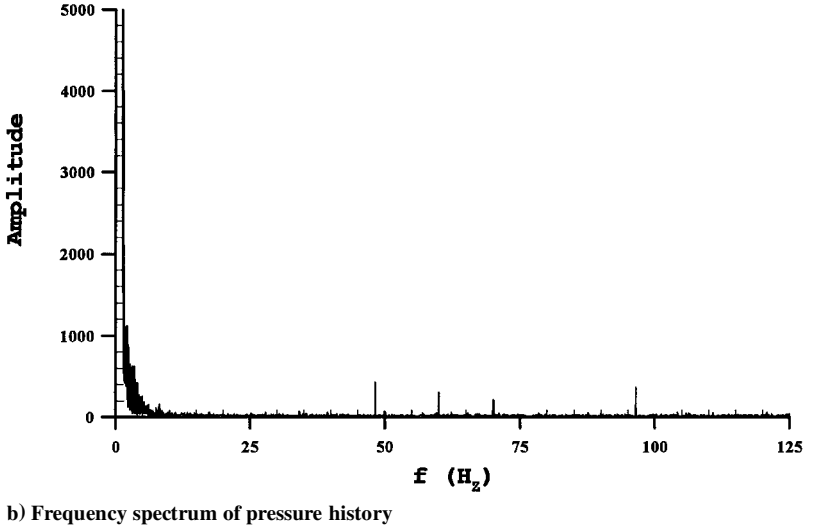

b) Frequency spectrum of pressure history

Fig. 6 Results of motor 2.

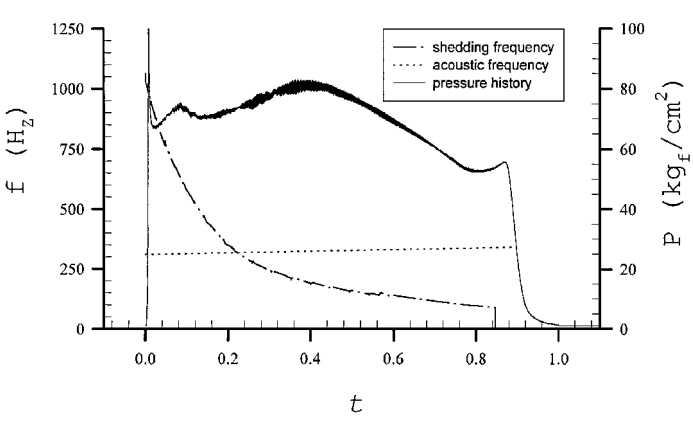

a) Pressure history and calculated frequencies

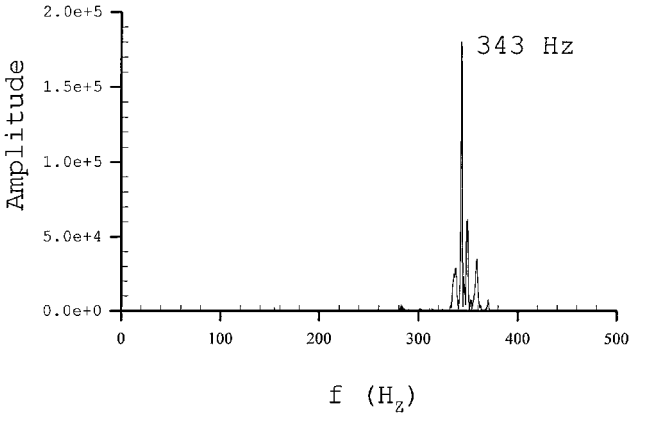

b) Frequency spectrum of pressure history

Fig. 7 Results of motor 3.

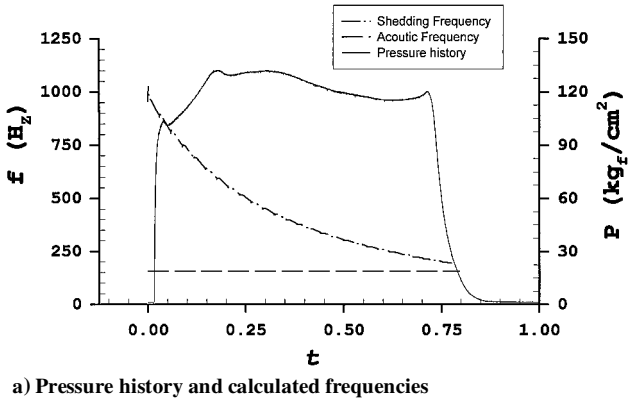

a) Pressure history and calculated frequencies

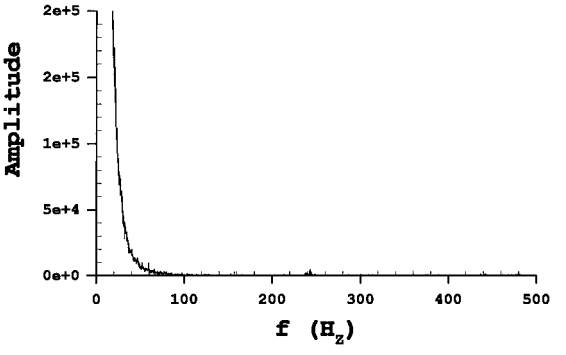

b) Frequency spectrum of pressure history

Fig. 8 Results of motor 4.

next vortex. Thus, according to Rayleigh's criterion, the oscillating amplitude may be amplified. This mechanism of the excitation of acoustic modes by vortex shedding is similar to that proposed by Culick and Magiawala[8] as well as by Dunlap and Brown.[9]

Figure 6 shows the results of motor 2. Unlike motor 1, motor 2 is designed for the requirement of two-phase thrust. The division of booster and sustainer phases is at $t = 0.388$. For convenience, two piecewise constant combustor pressures are used in these two phases. The corresponding wall blowing velocities are equal to 1.866 and 2.803 m/s for the booster and the sustainer phases, respectively. The higher blowing velocity in the sustainer phase is due to the much lower gas density (2.3864 kg/m^3 compared to 6.5066 kg/m^3 for booster phase). The discontinuous variation of the vortex shedding frequency as shown in Fig. 2a resulted from the assumption of piecewise constant ballistic parameters in two phases. It is found the natural vortex shedding frequency is near that of the acoustic oscillation just after ignition, but the discrepancy enlarges with time. The static test data of motor 2 agrees with the present predicted results because no apparent pressure oscillation and dominant frequency are found during the combustion period.

Motor 3 is designed for a single-phase booster whose mean gas density and blowing velocity are calculated to be 7.45 kg/m^3 and 7.543 m/s, respectively. Figure 7 shows the results of motor 3. One can observe significant pressure oscillation occurs at about $t = 0.2$, with a maximum amplitude about 3.6% of its magnitude and a dominant frequency of 343 Hz. It is encouraging that the two calculated frequency lines, as expected, coincide at $t = 0.22$ and $f = 322$. Similar to motor 1, the pressure oscillations also sustain for a certain period.

Motor 4 is also a single-phase booster with mean gas density of 10.44 kg/m^3 and gas blowing velocity of 3.19 m/s. The results of motor 4 are shown in Fig. 8. With the maximum values of L/D and $L1/L2$ among the five test motors, the fundamental acoustic frequency based on $4L1$ yields a lowest value (170 Hz). No apparent oscillation and frequency in the measured pressure record can be observed during the total action time, as shown in Fig. 8a. The analysis confirms this result because the calculated vortex shedding frequencies are always higher than those of the acoustic mode.

Note that although no combustion instability was reached from the preceding analysis for both motors 2 and 4, one can observe opposite trends between the two calculated frequencies. This implies that, to avoid the acoustic combustion instability in these SRMs with internal vortex shedding flowfield, the natural vortex shedding frequencies should be always larger or less than those of the quarter-wave acoustic mode of the upstream port. In our experience, for a motor predicted to be unstable, such as motor 1 or motor 3, it is difficult to get rid of the combustion instability by a small adjustment of motor dimensions. The reasons are limited shift in vortex shedding or acoustic frequencies cannot avoid the crossing of these two frequency curves.

The last case, motor 5, is shown in Fig. 9. Also, it is a single-phase booster with mean gas density of 10.87 kg/cm^3 and blowing velocity of 4.098 m/s. Pressure oscillation is found within the early action period with a dominant frequency at 493 Hz. Again, the present analysis shows good agreement with the measurements because the two calculated frequency lines intersect at the point of $t = 0.18$ and $f = 480$ Hz. Note the maximum oscillatory amplitude in motor 5 is less than 1.8% of its magnitude, which is much lower than those that appeared in motor 1 and motor 3. As mentioned in Sec. I, in the earlier combustion period the vortices are confined in narrow slots, and their contribution to combustion instability may be less significant.

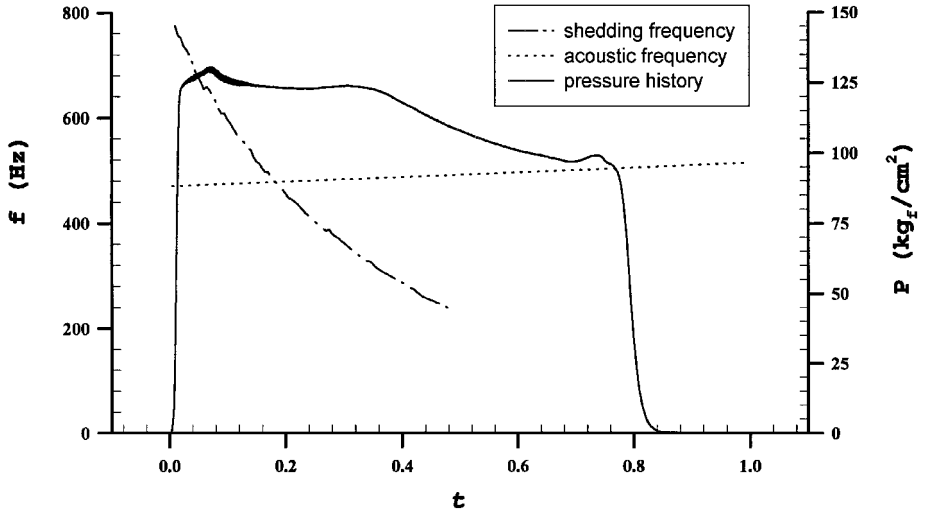

Pressure history and calculated frequencies

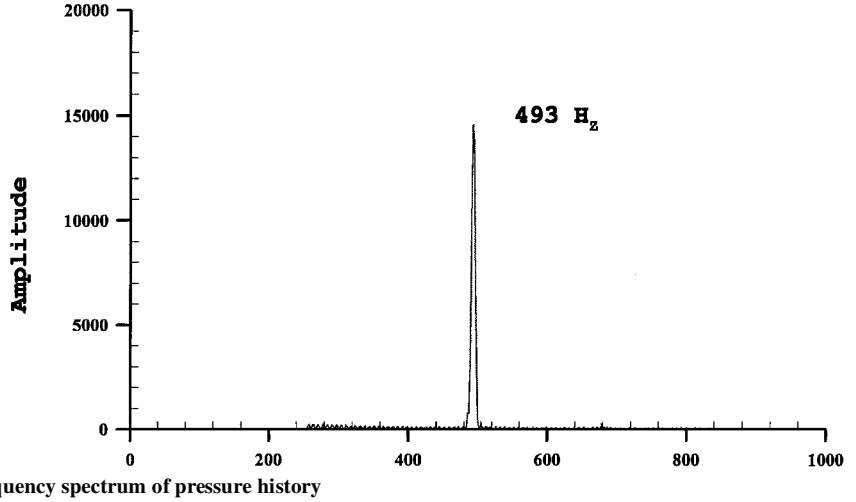

Frequency spectrum of pressure history

Fig. 9 Results of motor 5.

V. Conclusions

A numerical method to determine a sufficient condition of acoustic combustion instability in SRMs with slot-tube grain has been proposed. The basic concept is to compare the frequencies of vortex shedding and quarter-wave acoustic mode in the upstream port during the motor action time. To determine the vortex shedding frequencies, the flowfield of the upstream cylindrical port of the SRM with slotted-tube grain is solved by considering grain-surface regression. On the other hand, the acoustic frequencies are calculated based on the time-varying port length and the acoustic speed in the chamber, which is a function of the specific impulse. The method has been examined by analyzing five practical SRMs with slot-tube grain in which acoustic combustion instability occurs in three cases. The results indicate successful predictions for all five motors. Furthermore, in the analysis of motors 1, 3, and 5, good agreement is obtained between the measurements and predictions, not only for the oscillatory frequencies but also for the occurrence time.

The present study can only provide a sufficient condition of triggering acoustic combustion instability for SRMs with slotted-tube grain. When instability occurs, how serious the oscillating amplitude will become cannot be predicted by the present study. For instance, although the acoustic combustion instability is predicted to take place for motor 1, little can be asserted on the oscillation amplitude (3% in this case). This issue is very difficult and deserves further study.

Acknowledgments

The authors would like to thank to C.-S. Tsai and Y.-H. Hwang for reading their manuscript and giving helpful comments.

References

[1]Culick, F. E. C., "Stability of Three-Dimensional Motions in a Combustion Chamber," *Combustion Science and Technology*, Vol. 10, March 1975, pp. 109–124.

[2]Coates, R. L., and Horton, M. D., "Design Considerations for Combustion Stability," *Journal of Spacecraft and Rockets*, Vol. 6, No. 3, 1969, pp. 296–302.

[3]Lovine, R. L., and Waugh, R. C., "Standard Stability Prediction Method for Solid Rocket Motors," Vols. I–III, Aerojet Solid Propulsion Co., Air Force Rocket Propulsion Lab., Edwards AFB, CA, AFRPL-TR-76-32, 1976.

[4]Brown, R. S., Dunlap, R., Young, S. W., and Waugh, R. C., "Vortex Shedding as a Source of Acoustic Energy in Segmented Solid Rockets," *Journal of Spacecraft and Rockets*, Vol. 18, No. 4, 1981, pp. 312–319.

[5]Ma, Y., Van Moorhem, W. K., and Shorthill, R. W., "Experimental Investigation of Velocity Coupling in Combustion Instability," *Journal of Propulsion and Power*, Vol. 7, No. 5, 1991, pp. 692–699.

[6]Roh, T.-S., Tseng, I.-S., and Yang, V., "Effects of Acoustic Oscillations on Flame Dynamics of Homogeneous Propellants in Rocket Motors," *Journal of Propulsion and Power*, Vol. 11, No. 4, 1995, pp. 640–650.

[7]Flandro, G. A., and Jacobs, H. R., "Vortex-Generated Sound in Cavities," AIAA Paper 73-1014, Oct. 1973.

[8]Culick, F. E. C., and Magiawala, K., "Excitation of Acoustic Modes in a Chamber by Vortex Shedding," *Journal of Sound and Vibration*, Vol. 64, No. 3, 1979, pp. 455–457.

[9]Dunlap, R., and Brown, R. S., "Exploratory Experiments on Acoustic Oscillations Driven by Periodic Vortex Shedding," *AIAA Journal*, Vol. 19, No. 3, 1981, pp. 408–409.

[10]Schadow, K. C., and Wilson, K. J., "Characterization of Large-Scale Structures in a Forced Ducted Flow with Dump," AIAA Paper 85-0080, Jan. 1985.

[11]Dotson, K. W., Koshigoe, S., and Pace, K. K., "Vortex Shedding in a Large Solid Rocket Motor Without Inhibitors at the Segment Interfaces," *Journal of Propulsion and Power*, Vol. 13, No. 2, 1997, pp. 197–206.

[12]Flandro, G. A., "Vortex Driving Mechanism in Oscillatory Rocket Flows," *Journal of Propulsion and Power*, Vol. 2, No. 3, 1986, pp. 206–214.

[13]Vuillot, F., "Vortex-Shedding Phenomena in Solid Rocket Motors," *Journal of Propulsion and Power*, Vol. 11, No. 4, 1995, pp. 626–639.

[14]Kourta, A., "Acoustic-Mean Flow Interaction and Vortex Shedding in Solid Rocket Motors," *Internal Journal for Numerical Method in Fluids*, Vol. 22, No. 6, 1996, pp. 449–465.

[15]Kailasanath, K., Gardner, J. H., Boris, J. P., and Oran, E. S., "Computational Studies of the Effects of Acoustics and Chemistry on the Flow Field in an Axisymmetric Ramjet Combustor," CPIA 457, Vol. 1, Chemical Propulsion Information Agency, Laurel, MD, 1986, pp. 509–520.

[16]Kailasanath, K., Gardner, J. H., Boris, J. P., and Oran, E. S., "Interactions Between Acoustic and Vortex Structures in a Central Dump Combustor," *Journal of Propulsion and Power*, Vol. 3, No. 6, 1987, pp. 525–533.

[17]Bauwens, L., and Daily, J. W., "Flame Sheet Algorithm for Use in Numerical Modeling of Ramjet Combustion Instability," *Journal of Propulsion and Power*, Vol. 8, No. 2, 1992, pp. 264–269.

[18]Zaman, K. B. M. Q., and Hussain, A. K. F. M., "Vortex Paring in a Circular Jet Under Controlled Excitation. Part 1. General Jet Response," *Journal of Fluid Mechanics*, Vol. 101, Dec. 1980, pp. 449–491.

[19]Michalke, A., "On Spatially Growing Disturbances in an Inviscid Shear Layer," *Journal of Fluid Mechanics*, Vol. 23, Nov. 1965, pp. 521–544.

[20]Kim, Y. M., Chen, Z. P., Chen, C. P., and Ziebarth, J. P., "Pressure-Based Method for Combustion Instability Analysis," *Internal Journal for Numerical Methods in Fluids*, Vol. 19, No. 11, 1994, pp. 981–995.